physica status solidi rrl
www.pss-rapid.com

Pulsed Laser Ablation in Liquid: Numerical Evaluation of Laser Fluence

Cristiano Lo Pò, Francesco Ruffino,* Maria Grazia Grimaldi, and Stefano Boscarino*

Pulsed laser ablation in liquid is a very powerful technique that allows to synthesize colloidal solution of nanoparticles, starting from a target and a solvent, without waste. The performance of this process in terms of ablated mass per time depends on the laser fluence, the energy delivered per unit (or effective) area. Experimentally fluence evaluation is a tedious and indirect process, since the optical path passes through a lens and through an air–liquid interface, which is not easy to observe. In this work, a computational approach that provides the experimental parameters is developed, the laser ray paths inside the experimental apparatus are drawn, and the effective fluence on the target surface is evaluated. It aims to be an instrument to make predictions and help in the experimental setup tuning; moreover, the data obtained fit the theory developed for picosecond laser. The predictions can be extended to various real situations like a rotating fluid with a nonplane air–liquid surface.

1. Introduction

Pulsed laser ablation in liquid (PLAL) is a versatile and green technique for nanoparticles (NPs) production. It consists of the exploitation of a pulsed laser (from nanosecond to femtosecond) focused toward a target immersed in a liquid. Various experimental configurations are proposed, but the phenomena behind the whole process are always the same.[1,2] Once the laser pulse hits the target, a plasma plume is formed and some atoms of the target are ejected and arranged in NPs, usually of some nanometers radius but also some bigger particles are produced. The formation of plasma locally heats both the target and the solvent that vaporizes, forming a cavitation bubble. The presence of both solvent, vapors, and target atoms in the cavitation bubble can lead to the formation of various composites depending on the solvent. Platinum and gold are reported to be always metallic, but the presence of an organic solvent (methanol, ethanol or acetone) leads to the formation of a graphitic shell around the NPs.[3,4] For transition metals, the ablation in deionized (DI) water leads to the formation of oxide NPs,[5–7] while organic solvents lead to metallic NPs with a shell of graphitic or amorphous carbon[5,8,9] and in some case also carbides.[3] In any case, what controls the amount of ablated material and the NPs composition is the fluence F defined as

$$F = \frac{E}{S} \qquad \left[\frac{\mathrm{J}}{\mathrm{cm}^2}\right] \tag{1}$$

where E is the energy pulse and S is the spot surface.

A comprehensive knowledge of the technique in terms of theory is still not available since a lot of physical and chemical process occur as a consequence of the laser–matter interaction within the liquid and different research groups study different aspects. For example some groups studied the fluence on the plasma plume behavior and how this affects the NPs composition, morphology, and so on.[10,11] Some groups also observed the effects of strong electric fields during the process.[12,13] Theory and experiments were developed together by some groups that studied the relation between picosecond laser and the hole left in the target and the ablate mass,[14–17] while other groups reported how multiple pulses on a same spot and incubation phenomena affect the productivity.[16,18,19]

The technique is fast and clean because the NPs are directly ejected into the liquid without environmental dispersion and the experimental apparatus does not require any special and high-cost system except for the laser (and obviously the protective glasses), a target, some optics, a lens, and a becker. The target can be used for a long time and the whole used solvent at the end of the process becomes a colloidal solution of NPs ready to be used and deposited on the required substrate with drop casting, spin coating, spraying, dip coating.[1]

C. Lo Pò, F. Ruffino, M. G. Grimaldi, S. Boscarino
Dipartimento di Fisica e Astronomia "Ettore Majorana"
Università di Catania
Via Santa Sofia 64, 95123 Catania, Italy
E-mail: cristiano.lopo@fa.unict.it; francesco.ruffino@ct.infn.it

F. Ruffino
Consiglio Nazionale delle Ricerche
Istituto per la Microelettronica e Microsistemi (CNR-IMM)
Via Santa Sofia 64, 95123 Catania, Italy

F. Ruffino
Research Unit of the University of Catania
National Interuniversity Consortium of Materials Science and Technology
Viale Andrea Doria 8 and Via Santa Sofia 64, 95123 Catania, Italy

M. G. Grimaldi
INFN Sez. Catania
Via Santa Sofia 64, 95123 Catania, Italy

The ORCID identification number(s) for the author(s) of this article can be found under https://doi.org/10.1002/pssr.202400348.

DOI: 10.1002/pssr.202400348

NPs produced by PLAL found applications in a lot of fields such as catalysis, sensing, plasmonic, electronics, energy storage, water treatment, photovoltaic, and so on.[1,2,5,9,20–25]

The massive use of the PLAL technique for NPs synthesis leads our research group to optimize the experimental setup in order to reach the maximum productivity (ablated mass per unit time) in the smallest time. To achieve this goal, we developed a software that, given in input some parameters of the experimental setup, evaluates the fluence on the target surface. The fluence evaluation is not so simple because after the laser beam passes the lens, first, it is converged toward the focal point, but then it has to pass through the air–liquid interface and so the refraction Snell's law must be applied.

The aim of this work is to develop a simple numerical algorithm that evaluates the fluence on the target by computing the laser optical path through the instrumental apparatus. The novelty of this instrument relies in its fast execution and versatility to real-life situations to help the operator to understand what is happening in the experimental apparatus. Starting from experimental measured parameters and observing the trend in the data (and the fit), it can be feasible making predictions on the ablated mass with respect to the effective fluence. In order to make it more realistic, and close to the real-life experimental scenario, different parameters were included like: different target shape, different solvents, different amounts of solvent in the becker (the height of the solvent between the surfaces of target and solvent), and rotating solvent. It aims to be an instrument to make predictions and helps in the experimental setup tuning, like achieving the same fluence, hitting the surface target, in different experimental conditions as reported before. Also some considerations coming from the picosecond laser–matter theory were used to fit the obtained data even if the experiment was conducted by a nanosecond laser, opening the road to future theoretical considerations.

2. Fluence Evaluation Algorithm

The algorithm, represented in **Figure 1**, was written in Wolfram Mathematica language and mixes some geometric and ray tracing considerations. The algorithm gets an input from the following parameters: beam power (Watt), repetition rate (Hertz), refractive indexes of air and liquid, initial beam radius (cm), focal length of lens (cm), lens height (cm), target height (cm), and liquid height (cm). These last three parameters are measured with respect to the working plane, as illustrated in **Figure 2**a. The refractive index for air is considered as $n_{air} = 1$ and the one for the liquid is taken from *refractiveindex.info* online database. The algorithm works considering a beam with cylindrical symmetry and displays what happens on a plane perpendicular to the line of view, so the various objects can be expressed as simple 1D functions.

The first step is to compute the effective distance between the lens and the liquid and between the lens and the target surface by simply subtracting the respective positions: $l = h_{lens} - h_{liquid}$ and $l_{tot} = h_{lens} - h_{target}$. Then the code sets up the various graphic objects and then proceeds to declare (as mathematical object) the equation for the beam in air and liquid considering the lens placed in the plane $x = 0$ and also the air–liquid surface $s(x)$ is declared as mathematical function.

$$\text{In Air}: \gamma_1(x, \phi, x_0) = \text{Tan}(\phi)(x - x_0) \tag{2}$$

$$\text{In Liquid}: \gamma_2(x, \phi, x_0, \gamma_0) = \text{Tan}(\phi)(x - x_0) + \gamma_0 \tag{3}$$

The input beam is considered as one formed by parallel rays with a distance r from the beam center and for every one the path is computed in a cycle using r as cycle variable. After the lens all the rays converge toward the focal point, so their angle is computed as

$$\alpha = \text{ArcCos}\left(\frac{r}{\sqrt{r^2 + f^2}}\right) \tag{4}$$

where f is the focal length. For every ray, a native software function is used to find analytically the point (x_0, γ_0) where beam equation intercepts the surface equation $\text{Solve}[\gamma_1(x, \alpha, r) = s(x)]$. Through some simply geometrical considerations the angle γ between the incident ray and the surface normal is computed as

$$\gamma = \frac{\pi}{2} - \alpha + \text{ArcTan}\left(\left.\frac{\partial s(x)}{\partial x}\right|_{x=x_0}\right) \tag{5}$$

Then Snell's law is applied and with geometrical considerations, visualized in Figure 2b, the angle for the second laser beam is computed as

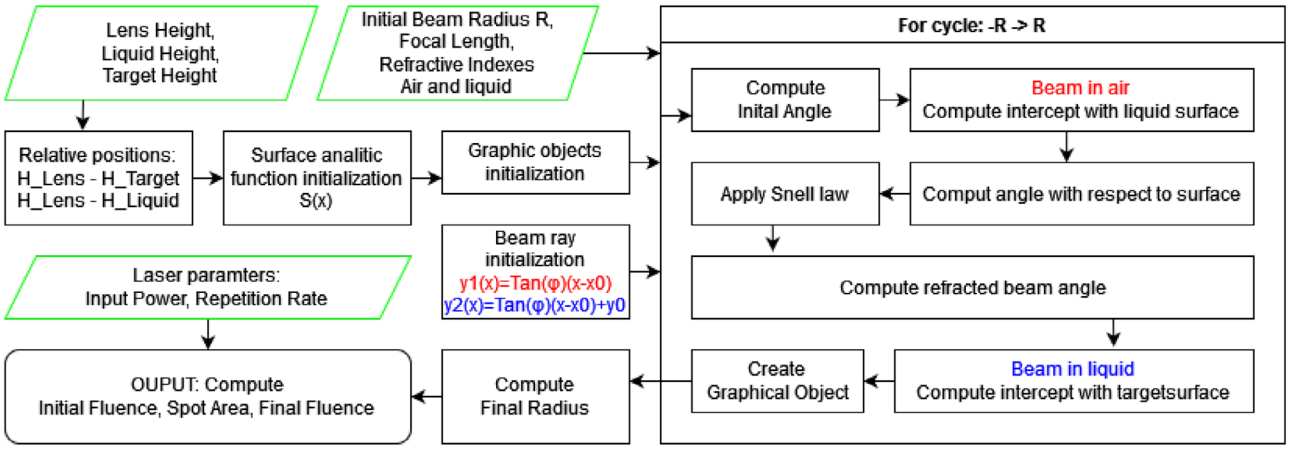

Figure 1. Scheme of the developed algorithm for the fluence evaluation.

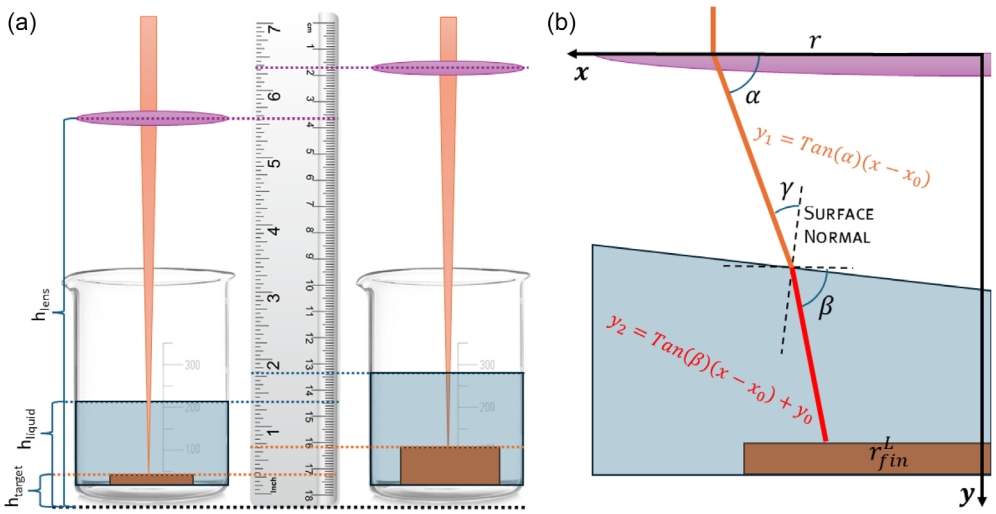

Figure 2. a) Visual representation of the motivation behind this work: various experimental setups with different liquid heights and target shapes requiring the same fluence. b) Visual representation of the formula reported in Section 2.

$$\beta = \frac{\pi}{2} - \mathrm{ArcSin}\left(\mathrm{Sin}(\gamma)\frac{n_{\mathrm{air}}}{n_{\mathrm{liquid}}}\right) + \mathrm{ArcTan}\left(\left.\frac{\partial s(x)}{\partial x}\right|_{x=x_0}\right) \tag{6}$$

The final beam position on the target r_{fin} is computed as before with a native software function using $\mathrm{Solve}[y_2(x,\beta,x_0,y_0) = -l_{\mathrm{tot}}]$, concluding the iterative part. At this point the fluence before and after is computed as

$$F = \frac{\mathrm{Power\ (W)/Repetition\ Rate\ (Hz)}}{\pi R^2} \tag{7}$$

where R is the beam radius and the spot is considered circular. For the initial fluence R is the initial beam radius, while, for the final fluence the radius was estimated as $\frac{r^{\mathrm{L}}_{\mathrm{fin}} - r^{\mathrm{R}}_{\mathrm{fin}}}{2}$ for the outermost rays on the left $r^{\mathrm{L}}_{\mathrm{fin}}$ and on the right $r^{\mathrm{R}}_{\mathrm{fin}}$. All the rays are plotted with a Gaussian opacity to give an idea of what physically happens during the ablation and what is the optical path as reported in Figure 2a and **Figure 3**a. At the end the algorithm provides as output the spot area on the target and the final fluence.

2.1. Errors and Uncertainties

Additions have been made to the previous algorithm to make it capable to handle with experimental uncertainty. The measured heights (lens, target, and liquid) can easily be affected by a parallax error, as well as the measured laser power has a certain variability of few mW over time.

To handle with the experimental errors, the previous described code is iterated for any possible combination of the limit cases and at the end the final beam radius on the target surface is the mean value, where its uncertainty is the standard deviation of every radius obtained with the limit cases. To clarify: if there are two parameters $a \pm \Delta a$ and $b \pm \Delta b$ as initial parameters with uncertainty, the algorithm is executed for four different sets of initial parameters: $\{a + \Delta a, b + \Delta b\}$, $\{a + \Delta a, b - \Delta b\}$, $\{a - \Delta a, b + \Delta b\}$, and $\{a - \Delta a, b - \Delta b\}$ that lead to four different final radius, from which the code extracts mean and standard deviation. Ideally every input parameter can be declared with its uncertainty with the consequence of increasing the execution time since the main code must be iterated 2^n times where n is the number of parameters with uncertainty.

3. Theoretical Background for Picosecond Laser

In this section, we just collected and reported the theory from several literature works (cited later in this section) about the laser–matter interaction for picosecond lasers, while in the next section we used this theory to just fit the data obtained by our algorithm and experiment conducted with a nanosecond laser. This can be a bit confusing: we reported the theory for picosecond laser and used this for nanosecond ones. As reported in the Introduction, there is no theory available for nanosecond laser–matter interaction, we just used the only available one and found that it works at least for the effects studied and reported here.

For picosecond laser, the pulse is very short and leads to the so called "cold ablation"[1] because laser pulse duration is shorter than the heat diffusion time into the material and so only the irradiated area is involved in the process. Nanosecond pulses instead lead to "hot ablation" because the pulse is long enough to also melt the target around the laser spot.

Returning to picoseconds, the process starts with the ionization of the target atoms, ejecting the electrons that form the plasma plume.[14,15] With the aid of plasma, several atoms are ejected from the target, leaving a hole with a depth d as follows.[16,17]

$$d = d_0 Ln\left(\frac{F}{F_{\mathrm{th}}}\right) \tag{8}$$

where d_0 is the light penetration depth, F is the fluence, and F_{th} is the threshold fluence, under which only radiation occurs without ablation. Even if this equation is derived from the theoretical

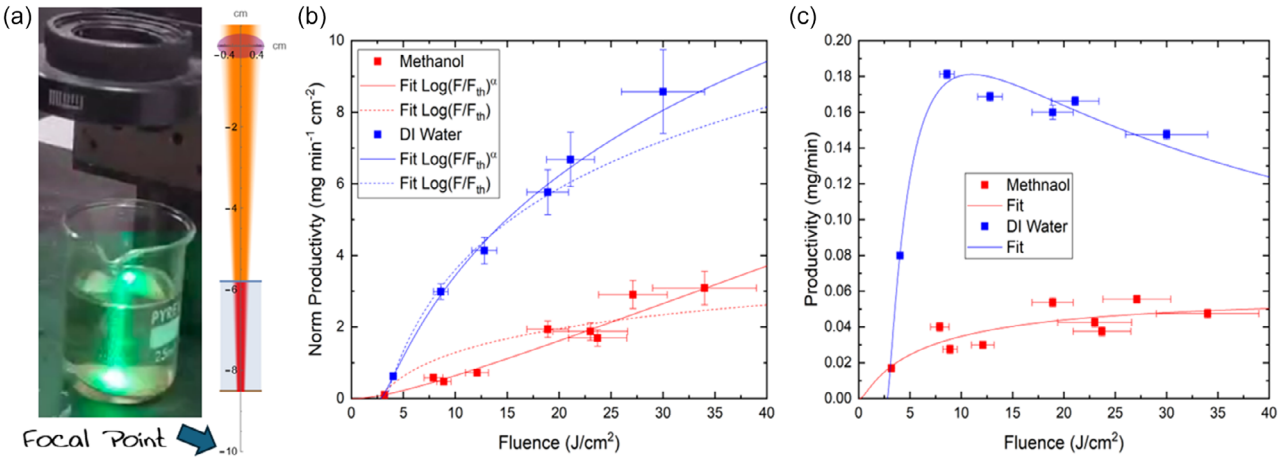

Figure 3. a) Real and computed optical path in the experimental apparatus. In the image the laser beam ($\lambda = 1064$ nm) appears green ($\lambda = 532$ nm) because the intensity is so high to induce double-photon phenomena with the NPs dispersed in solution. b) Normalized productivity (defined as mass ablated per time per spot area) versus fluence on the target surface. Data in methanol and DI water and best fits with two different functions $Ln(F/F_{th})$ and $Ln(F/F_{th})^{\alpha}$. c) The same data and best fits plotted as productivity (mass per minute) versus fluence.

consideration on picosecond pulses, it is quite general since it involves few parameters and does not have an explicit dependence on the pulse length. So, we decided to use the consequence of this formula to fit our experimental and computed data.

Assuming the laser beam has a Gaussian shape, also the effective fluence should have a Gaussian expression.

$$F = F_0 \exp\left(-\frac{r^2}{a^2}\right) \tag{9}$$

Ablation volume obtained by integrating Gaussian shape weighed by penetration depth is ref. [16]

$$V = \pi a^2 d_0 Ln\left(\frac{F}{F_{th}}\right) \tag{10}$$

Ablated mass per pulse follows the material density ρ[17]

$$M = \rho V = \rho \pi a^2 d_0 Ln\left(\frac{F}{F_{th}}\right) \tag{11}$$

This logarithm dependence is valid for a single pulse, some works about trenches dug with the laser[16] and short sequences of pulses[18] report a dependence of $Ln\left(\frac{F}{F_{th}}\right)^{\alpha}$ with $\alpha > 1$; this depends on the hole geometry but also on incubation phenomena[14,19] that happen at hole edges where the fluence is enough to melt the substrate, but less than F_{th}, so there is no ablation.

4. Experimental Section

The laser used for the experiments was a Quanta-Ray Pro Series Nd:YAG laser with $\lambda = 1064$ nm, 10 ns pulses, and $M^2 \approx 20$.[26] The repetition rate was set to 10 Hz and the mean power was measured with a Newport 818P-030-18H sensor read by a Gentec SOLO PE energy meter. The beam size was measured by shooting a single pulse on photographic paper, resulting in 0.5 cm radius. The used lens had a declared focal length of 10 cm. A visual comparison between the experiment and computation is given in Figure 3a.

Various ablation processes were performed on copper target employing DI water and methanol, the parameters and other details were optimized based on our previous works,[5,9,23] using at least 8 mL of solvent and performing the process for maximum 8 min to avoid to reach NPs concentration high enough to produce relevant scattering and absorption phenomena on the laser beam. For every experiment conducted, the ablated mass was measured by weighing the target before and after the ablation with a Sartorius ME5 microbalance (0.01 mg sensitivity), while the spot area on the target and the fluence were given by the algorithm described in Section 2. The results are reported in Figure 3b, it shows an initial linear behavior that tends to saturate at higher fluences. In the graph the fluence versus the ablate mass normalized by surface was reported during the experiments and the final beam area was variable. So Equation (11) becomes

$$\frac{\text{Mass}}{\text{Surface}} \propto Ln\left(\frac{F}{F_{th}}\right)^{\alpha} \tag{12}$$

Both this function and the logarithm with fixed $\alpha = 1$ were used for fitting the experimental data leading to the results reported in **Table 1**. Employing the logarithm with $\alpha = 1$ did not fit the data both with water and methanol, indicating that in the nanosecond experiment more phenomena take place; therefore, Equation (11) must be used. By fitting the data, for copper in DI water, F_{th} resulted in ≈ 2.8 J cm^{-2} with an exponent $\alpha = 1.4$, within the same range found in other works[16,18] with picosecond lasers. In methanol, the behavior was completely different, since the normalized productivity rose up slowly with the fluence and the fit resulted in $F_{th} \simeq 0.03$ J cm^{-2} and $\alpha \simeq 0.8$. Solvents with carbon atoms were reported in the pyrolysis process on hot metal surfaces[27] and so the formation of carbon-based products on the target surface strongly affected the

Table 1. Reuslt of fitting experimental data with the function Mass/Surface $\propto \ln(F/F_{th})^{\alpha}$.

Solvent	F_{th} [J cm^{-2}]	Exponent α
Methanol	2.6	1 (Fixed)
DI water	3.3	1 (Fixed)
Methanol	0.03	8.1
DI water	2.8	1.4

process. The presence of this carbon-based product is observed also around the produced NPs, how we reported in our previous works,[5,9] and, also, in literature.[8] In methanol (and any other organic solvent), the data showed certain variability since this kind of substance can easily take fire and, due to safety measurements, the experiment must be stopped and restarted several times to achieve the required ablation time.

The curves fit in the previous way can be transported in a fluence versus productivity graph, as shown in Figure 3c, where Equation (11) becomes

$$\text{Mass} \propto \frac{1}{F} Ln\left(\frac{F}{F_{th}}\right)^{\alpha} \tag{13}$$

the term $1/F$ comes from the definition of fluence $F = E/S$ that inversely depends on the surface at fixed energy. This graph is very helpful in experiments design and also for the technique scalability. In DI water, the trend had a peak of maximum productivity around 11 J cm^{-2} and then goes down, since Equation (13) has a maximum at $F = F_{th}\mathbf{e}^{\alpha}$. Data referred to methanol follows the same equation but with different parameters and smooth behavior. The peak was expected at ≈100 J cm^{-2} but this value was not realistic to observe since at higher fluence than the range explored in this work, the solvent instantly took fire.

So with the algorithm reproduced in this work we were able to fast evaluate the beam area on the target and the fluence and we found out that the results obtained by the theoretical consideration on PLAL using picosecond lasers were still valid in the same process using nanosecond lasers. Moreover this result was performed in a fast and rapid way without experimentally measuring the hole size on the target.

4.1. Independence of the Target Shape

The data reported in figure refer to ablation executed on an industrial copper target (99.999% purity) with a flat polished surface, see Supporting Information for the target and its SEM images. Some experiments were also conducted using a recycled commercial copper wire as target.[20] A short part of this wire used for domestic electrical connections in wall sockets was stripped of its insulating coating and pressed in a disk-like shape, see supplementary materials for the produced target and its SEM images. Before the ablation, it was cleaned with an ultrasonic bath in isopropyl alcohol for 15 min.

The data of fluence versus normalized productivity are reported in **Figure 4**a as pink points. Although these points stayed below the previous ones in the chart, they still followed the trend. This occurred because some of the produced NPs stayed trapped between the wires, and on their surface, as shown by SEM in Supporting Information; this is the reason why the ablated mass measured was less than the real one.

The entire algorithm and consideration can be applied to the generic nonuniform target surface; in fact, the final laser spot measured few millimeters and the effective part of the beam that induced the ablation measured some micrometers as observed by scanning electron micrscopy (SEM) images in Supporting Information. In addition we used an experimental setup with fixed target with the laser digging always in the same point and at the end the hole shape is the same independently of the surface morphology.

4.2. Rotating Experimental Apparatus

In some works, laser ablation is performed on rotating support or with the liquid moved by a magnetic stirrer[1] to achieve a better NP dispersion and avoid reirradiation phenomena of the NPs. The nonstatic condition leads to a nonflat liquid surface, in particular for rotating fluid the surface has a parabolic shape[28] with equation

$$y(x) = h_0 + \frac{\omega^2}{2g} x^2 \tag{14}$$

where h_0 is the height of the parabola minimum, ω is the angular velocity, and g is the gravitational acceleration. This surface acts as a divergent lens and spreads the beam as visualized in Figure 4b, since the angle for the Snell's law must be considered between the ray and the surface normal that is changing with the position. An experiment was conducted with 20 mL of rotating methanol and the industrial copper target and the following surface equation was used for computation.

$$s(x) = -l + Ax^2 \text{ [cm]} \tag{15}$$

with l the height in centimeter of the bottom of the parabola and A the measured parabola amplitude. The fluence evaluated with the algorithm without considering the effects of the rotating fluid was 24 J cm^{-2}, while taking into account the parabola surface in which the beam spread the fluence reaching a lower value of 9 J cm^{-2}. These two points were included in the graph in Figure 4a as blue triangles and the one computed with the beam spread in relation to the parabola shape fits with the previous data.

The possibility of defining an analytic function of the surface made the developed algorithm very adaptable to real-life situations. For example, Figure 4c reports a real life situation with the rotating becker voluntary misaligned, resulting in a complete change of direction of the laser path inside the liquid. By adding a displacement term x_d in the surface equation $s(x) = -l + A(x - x_d)^2$ the computed results recreated the experimental condition.

Another common situation that can be easily described by this algorithm is the static case in which the beam does not arrive perpendicular to the surface due to misalignment.

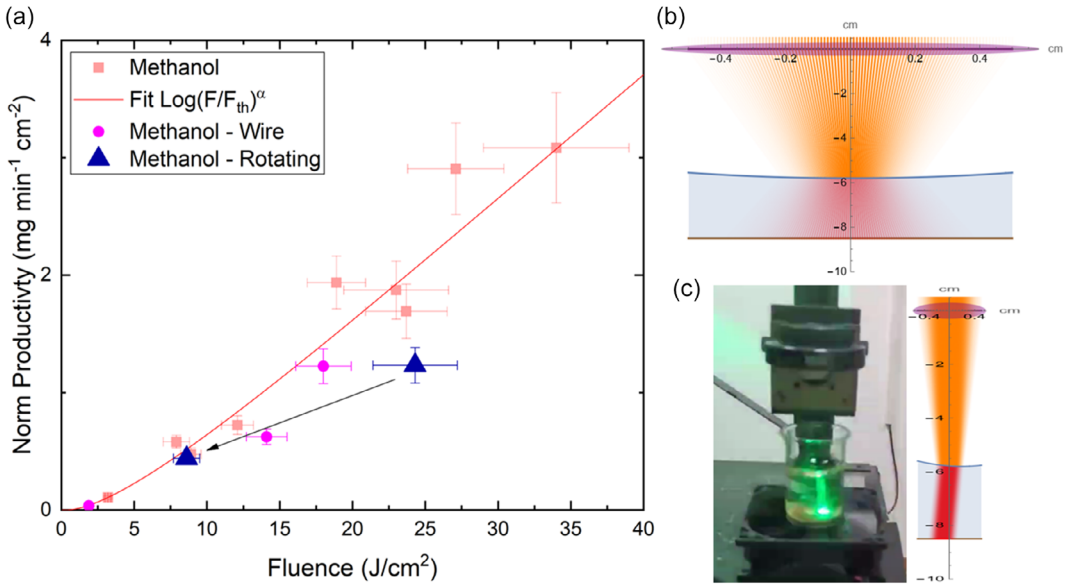

Figure 4. a) Rescaling of Figure 3b with focus on data produced in methanol and the fitting curve. In this graph are added the measurements with the rotating apparatus and also the ablation performed with Cu wire. b) Visual representation of the beam spreading passing through a rotating fluid surface (exaggerated situation). c) Real case of the algorithm working also with a beam not aligned with the parabola minimum, considering its lateral deviation also in real compared with a real case.

5. Conclusion

In conclusion, the tool that was initially developed like an experimental support has become a versatile instrument leading to several results that can be summarized as follows: 1) developing a rapid and functional tool for some experimental setup parameters to achieve the same fluence in various situation; 2) observing the same productivity with targets of the same material but with different shapes; 3) observing how a rotating fluid affects the beam path and its convergence; 4) observing a trend that matches with the theory and allows to make prediction on the productivity; 5) obtaining a visual representation of the laser optical path; 6) finding out that theory developed for PLAL with picosecon lasers is suitable for fitting data obtained with nanosceond lasers (further considerations require deeper theoretical studies).

This algorithm in its simplicity (<50 lines of codes) allows to extract a lot of information on the PLAL process, but this algorithm has the potentiality to be updated and improved taking in account other phenomena and provide a better understanding of the process. Moreover, the technique to evaluating the optical path can be extended in other systems that have an interface between two refractive indexes since the surface is expressed analytically and can find applications in other fields. We are planning future works to improve the algorithm by considering physical and chemical phenomena, like the thermal expansion, the chemical composition change and even the evaporation of the solvent, or a study on how the concentration of NPs produced during the process can absorb or scatter part of the laser beam decreasing the effective fluence over a prolonged time experiment, or even a study on how the fluence affects the plasma plume behavior and the NP size distribution. For future works we hope this simple algorithm we developed that only considers the optical path can be applied and will help in building a new knowledge about PLAL.

Supporting Information

Supporting Information is available from the Wiley Online Library or from the author.

Acknowledgements

This work was funded by European Union (NextGenerationEU), through the MUR-PNRR project SAMOTHRACE (grant no. ECS00000022). F.R., M.G.G., C.L.P. thank the support by the project "Multifunctional Hybrid Nanomaterials for Cancer Diagnosis and Personalized Target Therapy" through Programma di Ricerca di Ateneo UNICT 2024-26 linea 1. S.B. thanks the support by the project "Materiali Innovativi Per La Conversione dell'Energia Solare" through Programma di Ricerca di Ateneo UNICT 2024-2026 linea 1.

Open access publishing facilitated by Universita degli Studi di Catania, as part of the Wiley - CRUI-CARE agreement.

Conflict of Interest

The authors declare no conflict of interest.

Author Contributions

Cristiano Lo Pò: conceptualization (lead); data curation (lead); formal analysis (lead); investigation (lead); methodology (lead); software (lead); validation (lead); visualization (lead); writing—original draft (lead); writing—review & editing (equal). **Francesco Ruffino**: conceptualization (lead); data curation (lead); funding acquisition (lead); resources (lead); supervision (lead); writing—original draft (equal); writing—review & editing (equal). **Maria Grazia Grimaldi**: funding acquisition (equal); resources (equal); writing—review & editing (equal). **Stefano Boscarino**: conceptualization (equal); data curation (equal); investigation (equal); supervision (lead); validation (equal); writing—original draft (equal); writing—review & editing (equal).

Data Availability Statement

The data that support the findings of this study are available from the corresponding author upon reasonable request.

Keywords

fluences, nanoparticles, nanosecond lasers, pulsed laser ablation in liquids

Received: November 6, 2024
Revised: December 20, 2024
Published online:

[1] S. Barcikowski, V. Amendola, G. Marzun, C. Rehbock, S. Reichenberger, D. Zhang, B. Gökce, *Handbook of Laser Synthesis of Colloids*. **2016**. https://doi.org/10.17185/duepublico/41087.
[2] E. Fazio, B. Gökce, A. D. Giacomo, M. Meneghetti, G. Compagnini, M. Tommasini, F. Waag, A. Lucotti, C. G. Zanchi, P. M. Ossi, M. Dell'Aglio, L. D'Urso, M. Condorelli, V. Scardaci, F. Biscaglia, L. Litti, M. Gobbo, G. Gallo, M. Santoro, S. Trusso, F. Neri, *Nanomaterials* **2020**, *10*, 2317.
[3] D. Zhang, C. Zhang, J. Liu, Q. Chen, X. Zhu, C. Liang, *ACS Appl. Nano Mater.* **2018**, *2*, 28.
[4] J. Zhang, M. Chaker, D. Ma, *J. Colloid Interface Sci.* **2017**, *489*, 138.
[5] C. Lo Pò, F. Ruffino, A. Terrasi, E. Bruno, R. Reitano, M. G. Grimaldi, S. Boscarino, *J. Phys. Chem. Solids* **2024**, *193*, 112162.
[6] S. M. A. Aziz, U. M. Nayef, M. Rasheed, *Plasmonics* **2024**. https://doi.org/10.1007/s11468-024-02488-x.
[7] T. Begildayeva, D. Chinnadurai, S. J. Lee, Y. Yu, J. K. Song, M. Y. Choi, *J. Alloys Compd.* **2022**, *901*, 163446.
[8] T. Begildayeva, S. J. Lee, Y. Yu, J. Park, T. H. Kim, J. Theerthagiri, A. Ahn, H. J. Jung, M. Y. Choi, *J. Hazard. Mater.* **2021**, *409*, 124412.
[9] V. Iacono, C. Lo Pò, S. Scalese, S. Boninelli, G. G. Condorelli, M. G. Grimaldi, F. Ruffino, *APL Mater.* **2023**, *11*, 11.
[10] X. Li, W. Wei, J. Wu, S. Jia, A. Qiu, *J. Appl. Phys.* **2013**, *113*, 24.
[11] J. Wang, J. L. Zhao, J. L. Di, A. Rauf, W. Z. Yang, X. L. Wang, *J. Appl. Phys.* **2014**, *115*, 17.
[12] P. Liu, C. X. Wang, X. Y. Chen, G. W. Yang, *J. Phys. Chem. C* **2008**, *112*, 13450.
[13] X. Z. Lin, P. Liu, J. M. Yu, G. W. Yang, *J. Phys. Chem. C* **2009**, *113*, 17543.
[14] J. Krüger, W. Kautek, *Ultrashort Pulse Laser Interaction with Dielectrics and Polymers*, Springer, Berlin **2004**, pp. 247–290.
[15] M. Feit, A. Komashko, A. Rubenchik, *Appl. Phys. A* **2004**, *79*, 1657.
[16] J. Furmanski, A. M. Rubenchik, M. D. Shirk, B. C. Stuart, *J. Appl. Phys.* **2007**, *102*, 7.
[17] R. Intartaglia, K. Bagga, F. Brandi, *Opt. Express* **2014**, *22*, 3117.
[18] A. Žemaitis, P. Gečys, G. Račiukaitis, M. Gedvilas, *Proc. CIRP* **2020**, *94*, 962.
[19] H. J. Jung, M. Y. Choi, *J. Phys. Chem. C* **2014**, *118*, 14647.
[20] C. Lo Pò, S. Boscarino, S. Scalses, S. Boninelli, M. G. Grimaldi, F. Ruffino, Pulsed laser ablation of recycled copper: a new route toward sustainable plasmonic and catalytic nanostructures, Applied Surface Science Advances, Proof-Reading.
[21] S. Boscarino, V. Iacono, A. Lo Mastro, F. Tringali, A. Terrasi, M. G. Grimaldi, F. Ruffino, *Int. J. Mol. Sci.* **2022**, *23*, 11886.
[22] S. Boscarino, M. Censabella, M. Micali, M. Russo, A. Terrasi, M. G. Grimaldi, F. Ruffino, *Micromachines* **2022**, *13*, 247.
[23] C. Lo Pò, V. Iacono, S. Boscarino, M. G. Grimaldi, F. Ruffino, *Micromachines* **2023**, *14*, 2208.
[24] S. Boscarino, V. Iacono, A. Lo Mastro, S. Scalese, S. Boninelli, A. Scandurra, S. Lombardo, R. Corso, G. Guido Condorelli, R. Reitano, A. Terrasi, M. Grazia Grimaldi, F. Ruffino, *Appl. Surf. Sci.* **2024**, *655*, 159547.
[25] A. Scandurra, M. Censabella, S. Boscarino, G. G. Condorelli, M. G. Grimaldi, F. Ruffino, *Nanotechnology* **2021**, *33*, 045501.
[26] C. Awada, F. Ruffino, *Coatings* **2023**, *13*, 797.
[27] N. Lasemi, U. Pacher, C. Rentenberger, O. Bomatí-Miguel, W. Kautek, *ChemPhysChem* **2017**, *18*, 1118.
[28] P. Mazzoldi, M. Nigro, C. Voci, Fisica **2000**, ISBN 8836230679.